Astrophysical Journal, in press

A Radio Milli-Halo in the Nucleus of NGC 1275

C. S. Silver & G. B. Taylor
National Radio Astronomy Observatory,
P.O. Box 0, Socorro, NM 87801, USA

and

R. C. Vermeulen
Netherlands Foundation for Research in Astronomy,
P.O. Box 2, NL-7990 AA Dwingeloo, The Netherlands

ABSTRACT

We present high dynamic range (20,000:1 at 1414 MHz) VLBA observations of NGC 1275 (3C 84) at 1414 MHz, 612 MHz, and 330 MHz. With these observations, we have discovered a previously undetected counterjet component located ∼80 mas (20 h^{-1} pc) to the north of the compact core. This counterjet component, like those closer in to the nucleus, appears to be free-free absorbed. We have also discovered the first radio halo around an Active Galactic Nucleus on small (< 1 kpc) scales. This milli-halo cannot be the result of scattering, and is most likely produced by synchrotron radiation from relativistic particles that have diffused out from the parsec-scale jets over the lifetime of 3C 84.

Subject headings: galaxies:active — galaxies:individual(NGC 1275) — galaxies: jets — radio continuum: galaxies — galaxies:ISM — galaxies: nuclei — galaxies:halos

1. Introduction

The strong radio source 3C 84 is associated with NGC 1275, the dominant member of the Perseus cluster. Its proximity (z=0.0172) invites extensive study on all scales, and the bright core-dominated structure makes it a favorite calibrator source in the northern hemisphere. At z=0.0172, 1 mas = 0.24 h^{-1} pc, where $H_0 = 100\ h$ km s^{-1} Mpc^{-1}.

A pair of jets is observed in 3C 84 on scales ranging from <0.1 mas (<0.025h^{-1} pc) (eg., Dhawan *et al.* 1997) to >1 arcmin (>1.5h^{-1} kpc) (eg., Pedlar *et al.* 1990). In the mas-scale jets, velocities have been measured ranging from ∼0.3 mas yr^{-1} for the diffuse plasma (Romney *et al.* 1995) to ∼0.6 mas yr^{-1} for the knots (Marr *et al.* 1989). The predominant jet orientation is roughly North-South, but there is substantial curvature, particularly on the smallest and largest scales. The innermost core component has an inverted spectrum through 43 GHz, presumably due to synchrotron self-absorption (eg., Vermeulen *et al.* 1994). At successively lower frequencies, a progressively larger area further along the southern jet dominates the total flux density. On the largest scale, 3C 84 is surrounded by a 20′ (430 h^{-1} kpc) radio halo (Burns *et al.* 1992), as well as an X-ray halo extending as far as 1° (900 h^{-1} kpc; Fabian *et al.* 1981). Burns *et al.* classify this structure around 3C 84 as a mini-halo, based on its relatively small (<1 Mpc) size.

The southern jet is brighter than its counterpart on scales out to 20 arcsec. This is probably due in part to Doppler favoritism, but when independent VLBI observations at 8.4 GHz (Walker *et al.* 1994) and 22 GHz (Vermeulen *et al.* 1994) first revealed an inverted-spectrum feature ∼8 mas (2 h^{-1} pc) to the north of the core, it was realised that free-free absorption also plays a role, at least in the inner jets. Over a range of orientations, an equatorially flattened distribution of ionized gas (such as a disk or torus) can selectively hide the receding jet. Simultaneous multi-frequency observations to probe the structure of this plasma by measuring its free-free absorption as a function of radius have confirmed that the region ∼8 mas north of the core is optically thick at frequencies below ∼15 GHz (Walker *et al.* 1996, 1997). The intrinsic flux density ratio, revealed at 22 GHz, is ∼2:1, suggestive of only mildly relativistic jets (0.3–0.5 c) at a moderate (∼45°) angle to the line-of-sight (Vermeulen *et al.* 1994). Levinson *et al.* (1995) have shown that in order to maintain the required free-free opacity, there must be continuous exposure to the central source of ionizing radiation, as would be the case in the inner regions of a torus, or on the surface of a warped or flared disk, or on a flat disk with backscatter from a hot corona.

Recently, it was found that at 1.3 GHz the southern jet extends continuously from the core out to ∼100 mas (25 h^{-1} pc), showing that 3C 84 must have been active for the past few centuries (Taylor & Vermeulen 1996). There was also marginal evidence for a much fainter northern counterpart to this southern emission. Here, we report on a thorough investigation of the presence of emission out to hundreds of parsecs, using observations with the VLBA at low frequencies. In addition to establishing the presence of more counterjet emission, we have also discovered a sub-arcsecond-scale halo ("milli-halo") surrounding the entire core-and-jets structure.

2. Observations and Data Reduction

The observations were carried out at 330, 612, and 1414 MHz with the 10-element VLBA of the NRAO[1] in a single 12-hour observing session on 1995 October 23. The net integration time on 3C 84 was 160 minutes at 1414 MHz, and 250 minutes at each of 330 MHz and 612 MHz, spread over multiple snapshots to improve u,v coverage. At 330 MHz and 1414 MHz a total bandwidth of 8 MHz, split into 4 IF bands, was observed with 2-bit sampling for both right- and left-circular polarizations. Due to strong external interference at 612 MHz a 3.4 MHz passband filter was used on all antennas, so that only 2 IF bands contained usable data. The correlator produced a 2.06 second integration time and 32 channels per IF band.

Standard a priori flagging, amplitude calibration, fringe fitting, bandpass calibration, and frequency averaging procedures were followed in AIPS. All manual editing, imaging, deconvolution, and self-calibration were performed using DIFMAP (Shepherd, Pearson, & Taylor 1994, 1995). The two hands of polarization were added together for imaging, but were left separate in the self-calibration.

The naturally weighted 1414 MHz image of 3C 84 (Fig. 1) is our highest resolution image, and has a dynamic range of ~20,000 to 1. The origin was placed on the core by registering this image relative to a 5 GHz VLBA image (Romney *et al.* 1996). We assume the "core" to be the central bright component that appears in high-frequency images of the nucleus, in keeping with Romney *et al.* . Our lower frequency images were securely registered relative to 1414 MHz by using the distinct sequence of features (with changing flux density ratios) C, S1, S2, and S3, discussed below.

Total flux densities for the various features were measured by summing over rectangular windows, chosen on the 612 MHz image, and copied to 1414 MHz and 330 MHz. Component flux densities, dimensions of the windows used to measure them, and spectral indices are all listed in Table 1. The total flux density of the milli-halo was measured by windowing the flux surrounding the core. Note that for component NN we did not attempt to subtract the contribution from the overlapping milli-halo, which we estimate to be $\leq$1 mJy. The sum of the component flux densities agrees well with the total VLBA flux density at all three frequencies. These totals were compared to a VLA D-array spectrum taken just three days prior to our VLBA observation (R. C. Walker, private communication). At 330 MHz, the D-array beam includes too much extended flux, so the peak flux density in a 1988 VLA A-array observation was used instead; at this low frequency, variability in 7 years should not be a major concern. We used CTA 21 (B0316+16) as a calibrator and compared our VLBA flux densities to older single dish values. Spectral indices were calculated by tapering the higher-frequency image to the lower-frequency visibilities and convolving it with the lower-frequency beam size. We have concluded that our tabulated component flux densities are accurate to 10%, except for the milli-halo, which we estimate has uncertainties of ~30 mJy

[1]The National Radio Astronomy Observatory is operated by Associated Universities, Inc., under cooperative agreement with the National Science Foundation

at all frequencies. For the larger components, especially the milli-halo, it is likely that some flux density has been missed at the higher frequencies due to a lack of short spacings. The spectrum of the milli-halo could therefore be somewhat flatter.

TABLE 1

COMPONENT FLUX DENSITIES AND SPECTRA

Component	1414 MHz Jy	612 MHz Jy	330 MHz Jy	α(1414,612)	α(612,330)	Window mas×mas
C+S1	20.9 ± 2.1					38×38
S2	0.43 ± 0.04					43×20
C+S1+S2	21.4 ± 2.1	6.9 ± 0.7	4.7 ± 0.5	1.4 ± 0.4	0.6 ± 0.5	99×93
S3	0.40 ± 0.04	1.26 ± 0.1	1.30 ± 0.1	−1.3 ± 0.4	−0.1 ± 0.5	140×86
NN	0.027 ± 0.003	0.04 ± 0.004	0.011 ± 0.001	−0.5 ± 0.4	2.1 ± 0.5	72×54
Milli-Halo	0.08 ± 0.03	0.15 ± 0.03	0.23 ± 0.03	−1.0 ± 1.0	−0.7 ± 0.9	
Total	21.87	8.30	6.301			

3. Results

All flux densities and spectral indices are listed in Table 1, and they are plotted in Figure 5. We use the same jet component nomenclature as in Taylor & Vermeulen (1996). The brightest component, S1, appears at ∼10.5 mas (2.5 h^{-1} pc) south of the core (C), with which it is partly blended even at 1414 MHz. This region has a strongly inverted spectrum, and below 1414 MHz cannot be properly separated from component S2, which is ∼19 mas south of S1 (see Fig. 1), and also has an inverted spectrum.

Component S3, recently discovered by Taylor and Vermeulen (1996), consists of the extended emission centered at ∼75 mas (18 h^{-1} pc) south of the core along a position angle of ∼6°, with a diameter of ∼40 mas. This component has a steep spectrum above 612 MHz, and it probably turns over near ∼400 MHz, with a peak flux density of ∼1.3 Jy.

In the earlier 1347 MHz image (Taylor & Vermeulen 1996) the presence of a northern (counterjet) component could not be convincingly determined. At 612 MHz we now find a feature to be irrefutably present, and it also shows up clearly in the tapered 1414 MHz image (Fig. 2). We call it NN since it is not clear to us whether it can be matched to any feature in the southern jet. It is centered 80 mas (14 h^{-1} pc) to the north of the core along a position angle of ∼13°, and has a diameter of ∼35 mas (22 h^{-1} pc). NN was difficult to identify at 330 MHz and we used a tapered 612 MHz image to set the window to measure its flux density. Component NN seems to have a turnover frequency near ∼600 MHz, with a peak flux density of ∼40 mJy (Fig. 3).

We have discovered a milli-halo of diffuse emission surrounding all of the aforementioned features. The tapered 330 MHz image, with optimal sensitivity to large-scale emission, best demonstrates its extent (Fig. 4). We have also unequivocally found the milli-halo at 612 MHz by tapering to the beam of the 330 MHz image. Finally, an extreme taper of the 1414 MHz image also indicates some traces of the milli-halo, particularly in regions northwest and northeast of the core. With an average diameter of ∼500 mas (120 h^{-1} pc), the milli-halo is slightly elongated along the north-south direction, corresponding approximately to the orientation of the jet and counterjet. We note that the milli-halo may extend somewhat beyond this, but the observations are limited by the shortest available spacings of the VLBA. Our flux density measurements are based on tapered images at all three frequencies, and show that the region has a steep spectrum throughout ($\alpha \sim -0.9$), reaching a total flux density of 230 mJy at 330 MHz (Fig. 5).

4. Discussion

4.1. Overall Spectrum

Sijbring (1993) reported WSRT observations as showing a dip in the total flux density spectrum of the sub-arcsecond core at 612 MHz down to ∼5.5 Jy, and from it suggested the presence of a substantial component surrounding the cm wavelength VLBI core, with a flux density of several Jy, and peaking at ∼300 MHz. However, internal and external calibration gives us confidence in our measured total flux densities, which increase smoothly with frequency (∼8.3 Jy at 612 MHz), and can be understood simply from the sum of the components in our images. There is no evidence for a prominent sub-arcsecond sized component: the milli-halo only contains only a few hundred mJy.

4.2. The Jet Components

Walker *et al.* (1996, 1997), and Romney *et al.* (1996) have performed a multi-frequency VLBI imaging study of the inner counterjet ($\leq$10 mas), which shows that it is most likely free-free absorbed. We believe that the newly found feature NN is also affected by free-free absorption, since its large angular size and low brightness temperature rules out synchrotron self-absorption, just as was found for the inner counterjet (eg., Vermeulen *et al.* 1994). The equipartition angular size derived for NN from the spectrum assuming synchrotron self-absorption is only 1.7 mas (see Scott & Readhead 1977).

The free-free turnover frequency decreases with radius, as the obscuring matter gradually becomes less opaque; parameterizing $\tau_{\rm ff} \propto R^{-\eta}$, Walker *et al.* (1997) found $\eta \sim 2.2$. Using our new data on NN, we can estimate the radial dependence over a much larger range: the turnover frequency drops from ∼10 GHz at 8 mas from the core to ∼0.5 GHz at 80 mas from the core, so that $\eta \sim 2.6$, remarkably consistent with the number determined only from small scales. The free opacity is given by $\tau_{\rm ff} \approx 2.5 \times 10^{-7} \nu_9^{-2} L n_{\rm e}^2 T_4^{-3/2}$, where ν_9 is the observing frequency in GHz, L is the pathlength in pc, $n_{\rm e}$ the electron density in cm^{-3}, and T_4 the temperature in units of 10^4 K (e.g, Levinson *et al.* 1995). Thus, if one envisages an obscuring region of constant opening angle (a wedge-like disk, say) in which $L \propto R$, then for a constant temperature medium we find $n_{\rm e} \propto R^{-1.8}$. This dependence would be steeper if T were to fall off with radius. Conversely, $n_{\rm e}$ would fall off less steeply if the pathlength through the obscuring region would increase less than linearly with radius, as might happen for toroidal structures or gradually flattening disks. It is possible that the cooling flow of 200–400 $M_\odot$ y^{-1} deduced from X-ray observations (Fabian *et al.* 1981) results in an unusually thick disk.

Note that above we give only pure scaling arguments, which depend on the ratio of the turnover frequencies at the different radii. However, if we assume $T_4 = 1$, and take a pathlength of $L = 10$ pc towards NN (which is at a projected radius of $20h^{-1}$ pc), then the turnover frequency of ~0.5 GHz implies $n_{\rm e} \sim 300$ cm^{-3}.

The location of NN is not consistent when overlaying the 1414 and 612 MHz maps. This is probably an opacity effect due to the accretion disk that obscures the jet's extension at 612 MHz. The counterjet shows a similar effect at 22 and 8 GHz closer in to the nucleus (Romney *et al.* 1996).

It is tempting to identify NN as the counterpart of S3. In that case their projected distance ratio is nearly 1:1, substantially different from the 2:1 ratio suggested for the mas-scale jets. With this speculative association, and if the jets are still anti-parallel, then at $20h^{-1}$ pc they are either no longer at ~45° (Walker *et al.* 1994) to the line of sight, but nearly in the plane of the sky, and/or they have slowed down. However, their flux density ratio at 1414 MHz (above the turnover) is 15:1, not 1:1 as expected for a perfectly matching pair of knots. In short, we do not feel confident in identifying NN as the counterpart of any particular feature in the southern jet.

We note that the overall angular size of S3 (~40 mas) is also larger than the equipartition angular size of 17 mas predicted from the spectrum assuming synchrotron self-absorption. The mismatch would be worse if the observed flux density of S3 is increased by Doppler beaming. However, the highest resolution 1414 MHz image does show substantial substructure within S3, which is in fact remarkably similar to knottiness seen in S1 on much smaller scales (for example at 22 GHz, Vermeulen *et al.* 1994). Thus we believe it is quite possible that synchrotron self-absorption fully determines the flux densities in region S3.

4.3. The Milli-Halo

The milli-halo has a steep spectrum, in contrast to the embedded features which dominate the total flux density, and therefore the milli-halo is not due to Thompson scattered radiation, which is independent of frequency. Since the milli-halo has a brightness temperature $\sim 3 \times 10^7$ K, it is almost surely non-thermal, and we conclude that it is due to synchrotron emission. Under equipartition and minimum energy conditions, and adopting a path-length of 75 pc through a uniformly filled halo, we derive $B_{\rm me} \approx 200$ μGauss, and $u_{\rm me} \approx 4 \times 10^{-9}$ erg cm^{-3}. With this, the relativistic particle aging timescale is $t_{\rm loss} \approx 1.5 \times 10^5$ (3.2×10^5) yr at 1414 MHz (330 MHz). This timescale suggests a minimum velocity of 380 (180) km s^{-1} for particles to travel across the radius of the milli-halo. Assuming equipartition between the relativistic plasma and the thermal gas pressures, a temperature of $\sim 10^7$ K (Fabian *et al.* 1981) implies a gas density of ~ 1 cm^{-3}. Assuming that the material is primarily neutral hydrogen, the Alfvén velocity is ~ 430 km s^{-1}, which is reasonably close to the velocity required to supply relativistic particles to the edge of the source without requiring reacceleration. This may indicate that the size of the milli-halo is constrained by the Alfvén velocity. The real situation may be complicated, however, by magnetic fields that are tangled on scales smaller than the milli-halo. In this case Eilek (1991) demonstrates that diffusive transport can still transport relativistic particles up to 10s of kpc before they encounter severe synchrotron losses at frequencies of 1 GHz.

To produce the milli-halo, magnetic fields of strength ~ 200 μG are required. These magnetic fields may have been supplied by jet material expanding transversely to the predominantly north-south direction of the jet (as described in the evolutionary model of Eilek & Shore 1989). Alternatively, there is strong evidence from studies of Faraday Rotation Measures of cluster-center radio sources for magnetic fields associated with cooling flow clusters (Taylor & Perley 1993; Ge & Owen 1993; Taylor, Barton & Ge 1994). These cluster magnetic fields have strengths of order 10 μG, and coherence lengths of ~ 4 kpc, but at the very center of the cluster it is natural to expect that the cooling flow may increase the magnetic field strength (Soker & Sarazin 1990). 3C 84 itself exhibits unusually low fractional polarization (Aller *et al.* 1985; Ge & Roberts 1993), which may be the result of depolarization by a tangled Faraday screen.

It is interesting that Carilli, Wrobel, & Ulvestad (1997) have recently discovered evidence for a milli-halo with very comparable properties in Mrk 231. We agree with them that another possible origin for the milli-halo is from supernovae related to star formation from a disk or bulge in the inner $\sim$100 pc. To produce the observed luminosity of the milli-halo of $2.6 \times 10^{22} h^{-2}$ W Hz^{-1} at 1.4 GHz requires a high-mass star formation rate of 6.4 h^{-2} M$_\odot$ yr^{-1} (see Condon 1992). This is not an unusually large high-mass star formation rate and in fact higher rates are predicted by Scoville, Yun, & Bryant (1997) for the central accretion disks of systems like Arp 220 and Mrk 231. There is a well known correlation between the radio and infrared luminosity for normal galaxies (Condon 1992). Based on the IRAS 60 and 100 μm flux densities of 7.146 and 6.981 respectively this predicts $\sim 130 \pm 70$ mJy of emission at 1.4 GHz, in agreement with the 80 ± 30 mJy observed. We note, however, that the above formulation assumes that the AGN in 3C 84 makes no contribution to the IR flux densities, either directly, or indirectly through heating of the dust.

Finally, we note that the spectrum of the milli-halo is extremely straight between 1414 MHz and 330 MHz, in contrast to the curved spectrum of NN, which peaks at $\sim$600 MHz. This indicates that the milli-halo is outside the region of absorbing material that cuts off the spectrum of NN. We conclude, therefore, that the material that is responsible for the absorption of NN is located in the region between the milli-halo and the counterjet.

5. Conclusions

We present the discovery of a counterjet component located 80 mas to the north of the core in 3C 84. This counterjet is found to have a low-frequency turnover in its spectrum at $\sim$600 MHz, which may be explained in terms of free-free absorption by the outer parts of the equatorially flattened structure (disk or torus) thought to absorb the inner jets at higher frequencies.

We also present the first observation of a radio halo surrounding the core of an AGN at a radius of $\sim$250 mas (60 h^{-1} pc). We dub this structure a "milli-halo" since it is roughly 1000 times smaller than large-scale radio halos like the one in the Perseus cluster containing NGC 1275. It has only recently become possible to make VLBI images at 300 MHz with a dynamic range $>$ 1000:1, raising the prospect that future observations will reveal milli-halos around other compact sources as well.

The discovery of the milli-halo provides a new tool for understanding the conditions near the cores of AGNs. Such a structure around the nucleus indicates a repository of particle energies, possibly contributing to the overall luminosity of AGNs at low frequencies. There is recent evidence for a similar milli-halo around Mrk 231, indicating that such structures are not unique to 3C 84. High-sensitivity, low-frequency VLBI observations of other AGNs would be of interest in order to provide additional information about the physical properties of milli-halos.

The authors thank Craig Walker, Chris Carilli and Jean Eilek for helpful discussions. C. S. S. acknowledges support from the REU program of the NSF and assistance from the entire NRAO staff during a summer research position. This research has made use of the NASA/IPAC Extragalactic Database (NED) which is operated by the Jet Propulsion Laboratory, Caltech, under contract with NASA. This research has also made use of the United States Naval Observatory (USNO) Radio Reference Frame Image Database.

REFERENCES

Aller, H. D., Aller, M. F., Latimer, G. E., & Hodge, P. E. 1985, ApJS, 59, 513

Burns, J. O., Sulkanen, M. E., Gisler, G. R., & Perley, R. A. 1992, ApJ, 388, L49

Carilli, C. L., Wrobel, J. M., Ulvestad, J. S. 1997, AJ, in press

Condon, J. J. 1992, ARA&A, 30, 575

Dhawan, V., Kellermann, K. I., & Romney, J. D. 1997, submitted to ApJ

Eilek, J. A. 1991, in "Particle Acceleration in Cosmic Plasmas" eds. G.P. Zank & T.K. Gaisser (AIP: New York), p. 455

Eilek, J. A., & Shore, S. N. 1989, ApJ, 342, 187.

Fabian, A. C., Hu, E. M., Cowie, L. L., & Grindlay, J. 1981, ApJ, 248, 47

Ge, J.-P., & Owen, F. N. 1993, AJ, 105, 778

Ge, J.-P., & Roberts, D. H. 1993, BAAS, 183, 53.10

Levinson, A., Laor, A., & Vermeulen, R. C. 1995, ApJ 448, 589

Marr, J. M., Backer, D. C., Wright, M. C. H., Readhead, A. C. S., & Moore, R. 1989, ApJ, 337, 671

Pedlar, A., Ghataure, H. S., Davies, R. D., Harrison, B. A., Perley, R. A., Crane, P. C., & Unger, S. W. 1990, MNRAS, 246, 477 Romney, J. D. 1983, ApJ, 265, 107

Romney, J. D., Benson, J. M., Dhawan, V., Kellermann, K. I., Vermeulen, R. C., & Walker, R. C. 1995, PNAS, 92, 11360

Romney, J. D., Walker, R. C., Kellermann, K. I., Vermeulen, R. C., & Dhawan, V. 1996, in *IAU Symposium 175: Extragalactic Radio Sources* eds. R. Ekers, C. Fanti & L. Padrielli (Kluwer: Dordrecht) p. 27

Scott, M. A., & Readhead, A. C. S. 1977, MNRAS, 180, 539

Scoville, N. Z., Yun, M. S., Bryant, P. M. 1997, ApJ, 484, 702

Shepherd, M. C., Pearson, T. J., & Taylor, G. B. 1994, BAAS, 26, 987

Shepherd, M. C., Pearson, T. J., & Taylor, G. B. 1995, BAAS, 27, 903

Sijbring, D. 1993, PhD thesis (University of Groningen), p.43

Soker, N., & Sarazin, C. L. 1990, ApJ, 348, 73

Taylor, G. B., & Perley, R. A. 1993, ApJ, 416, 554

Taylor, G. B., Barton, E. J., & Ge, J.-P. 1994, AJ, 107, 1942

Taylor, G. B., Vermeulen, R. C. 1996, ApJ, 457, L69

Vermeulen, R. C., Readhead, A. C. S., & Backer, D. C. 1994, ApJ, 430, L41

Walker, R. C., Romney, J. D., & Benson, J. M. 1994, ApJ, 430, L45

Walker, R. C., Romney, J. D., Vermeulen, R. C., Dhawan, V., & Kellermann, K. I. 1996, in *IAU Symposium 175: Extragalactic Radio Sources* eds. R. Ekers, C. Fanti & L. Padrielli (Kluwer: Dordrecht) p. 30

Walker, R. C., Kellermann, K. I., Dhawan, V., Romney, J. D., Benson, J. M., Vermeulen, R.C., & Alef, W. 1997, in *IAU Colloquium 164: Radio Emission from Galactic and Extragalactic Compact Sources* eds. J. A. Zensus, G. B. Taylor and J. M. Wrobel (PASP: San Francisco) in press

This preprint was prepared with the AAS LaTeX macros v4.0.

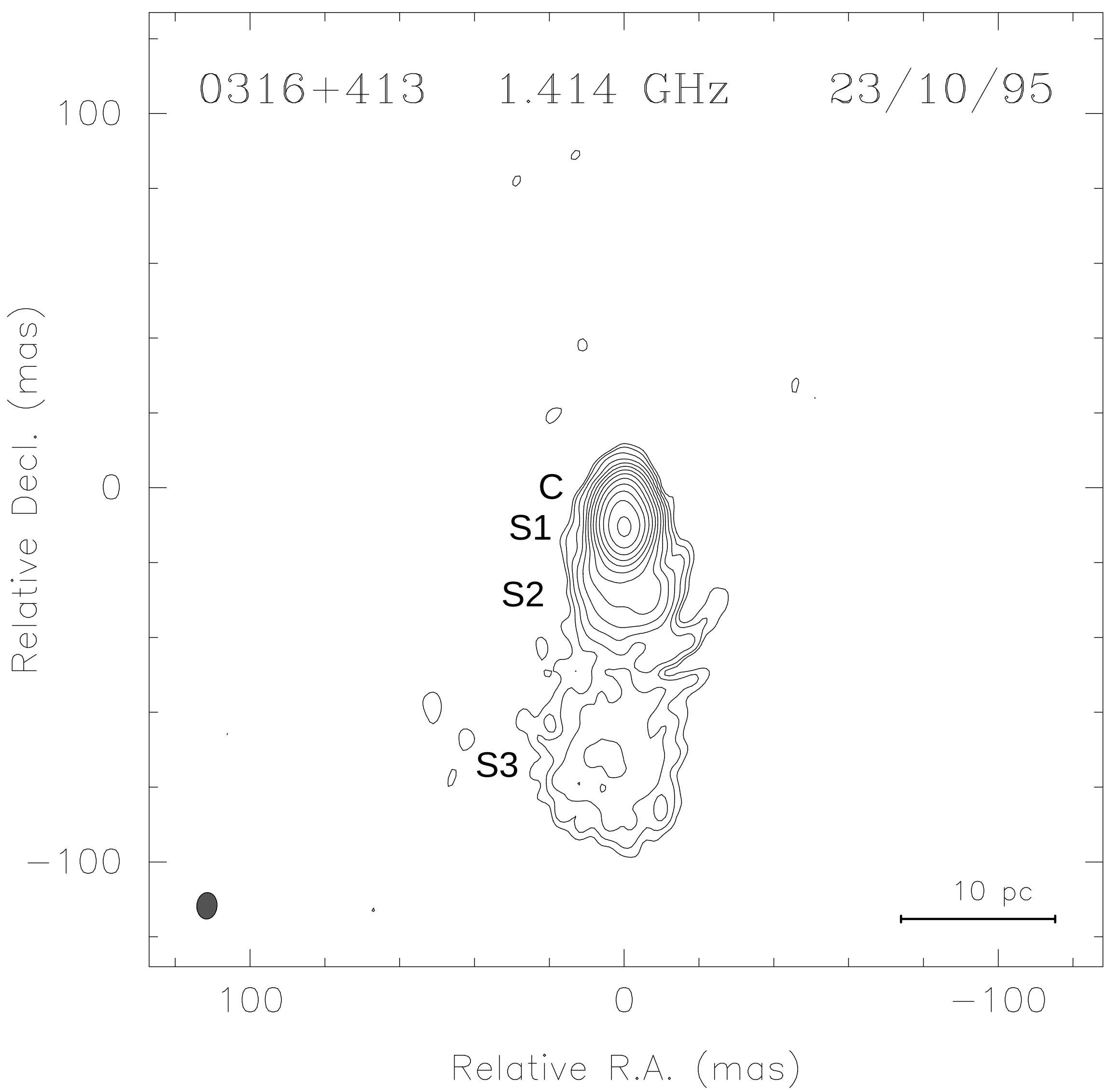

Fig. 1.— The naturally weighted image of 3C 84 at 1414 MHz. The restoring beam has dimensions 7.08×5.41 mas in position angle $-4.75°$. Contour levels are at 2, 4, 8, 16, 32, ... 8192 mJy/beam.

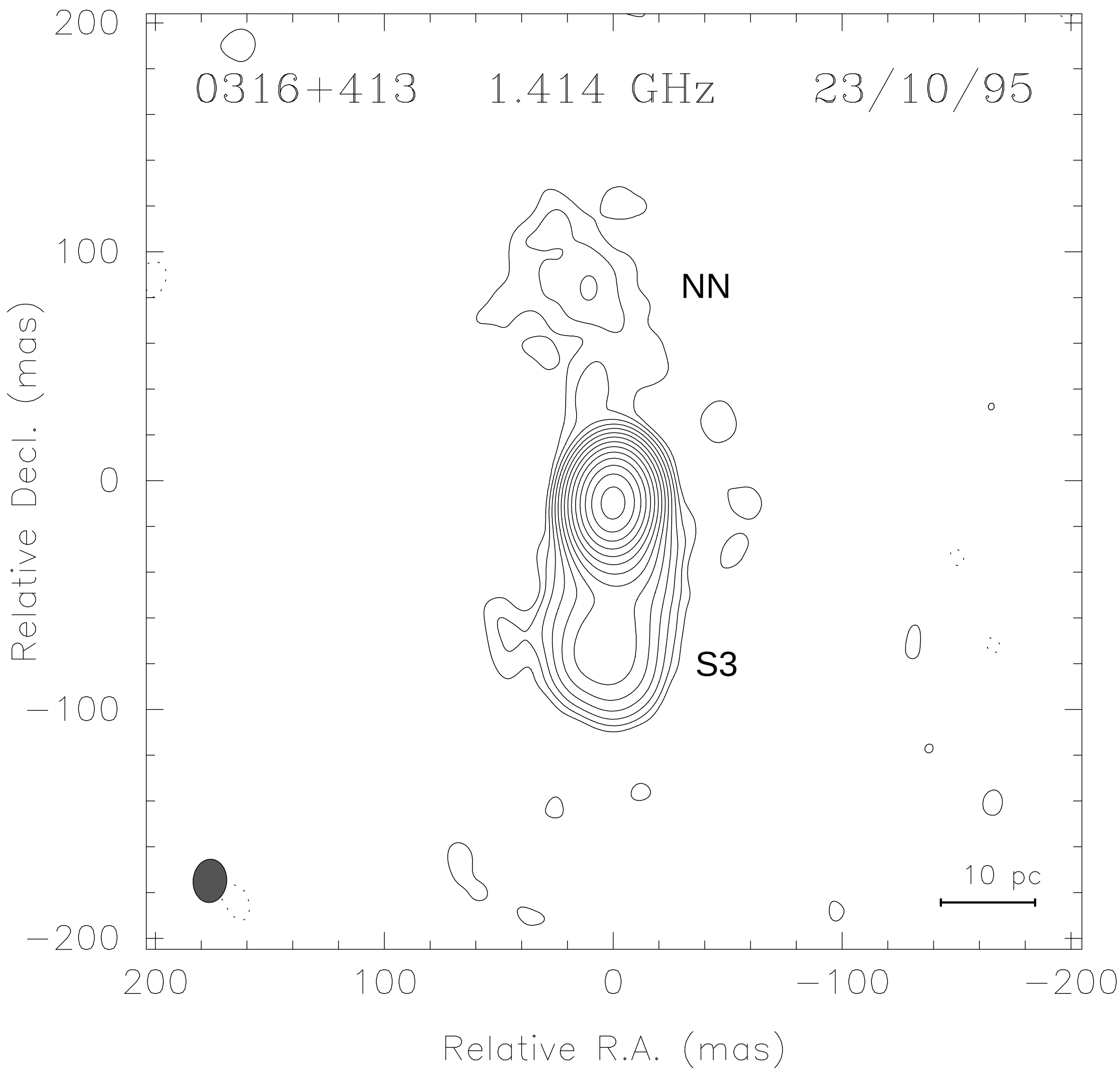

Fig. 2.— The naturally weighted and tapered image of 3C 84 at 1414 MHz. A Gaussian taper falling to 50% at 8 Mλ was applied and the image was restored with a beam of 18.9 $\times$ 14.7 mas in position angle $-4.64°$. Contour levels are at -1.7, 1.7, 3.4, 6.8, 13.6, ... 13107 mJy/beam with negative contours shown as dashed lines.

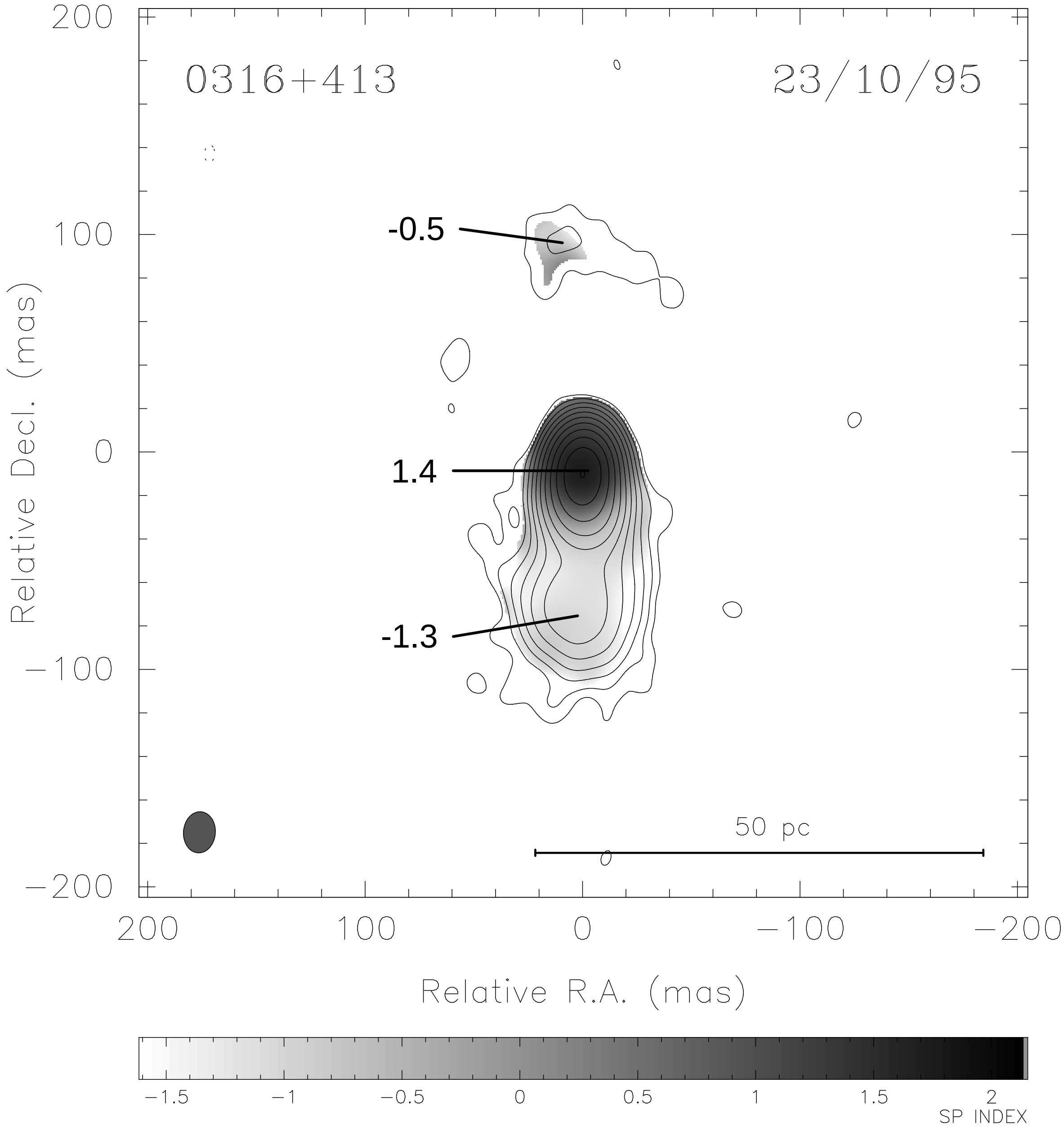

Fig. 3.— The spectral index image between the tapered 1414 MHz image and the naturally weighted 612 MHz image. The image is overlaid with contours of the naturally weighted 612 MHz image. The restoring beam has dimensions 18.9 $\times$ 14.7 mas in position angle $-4.64°$. Contour levels are at -4, 4, 8, 16, 32, ... 4096 mJy/beam with negative contours shown as dashed lines.

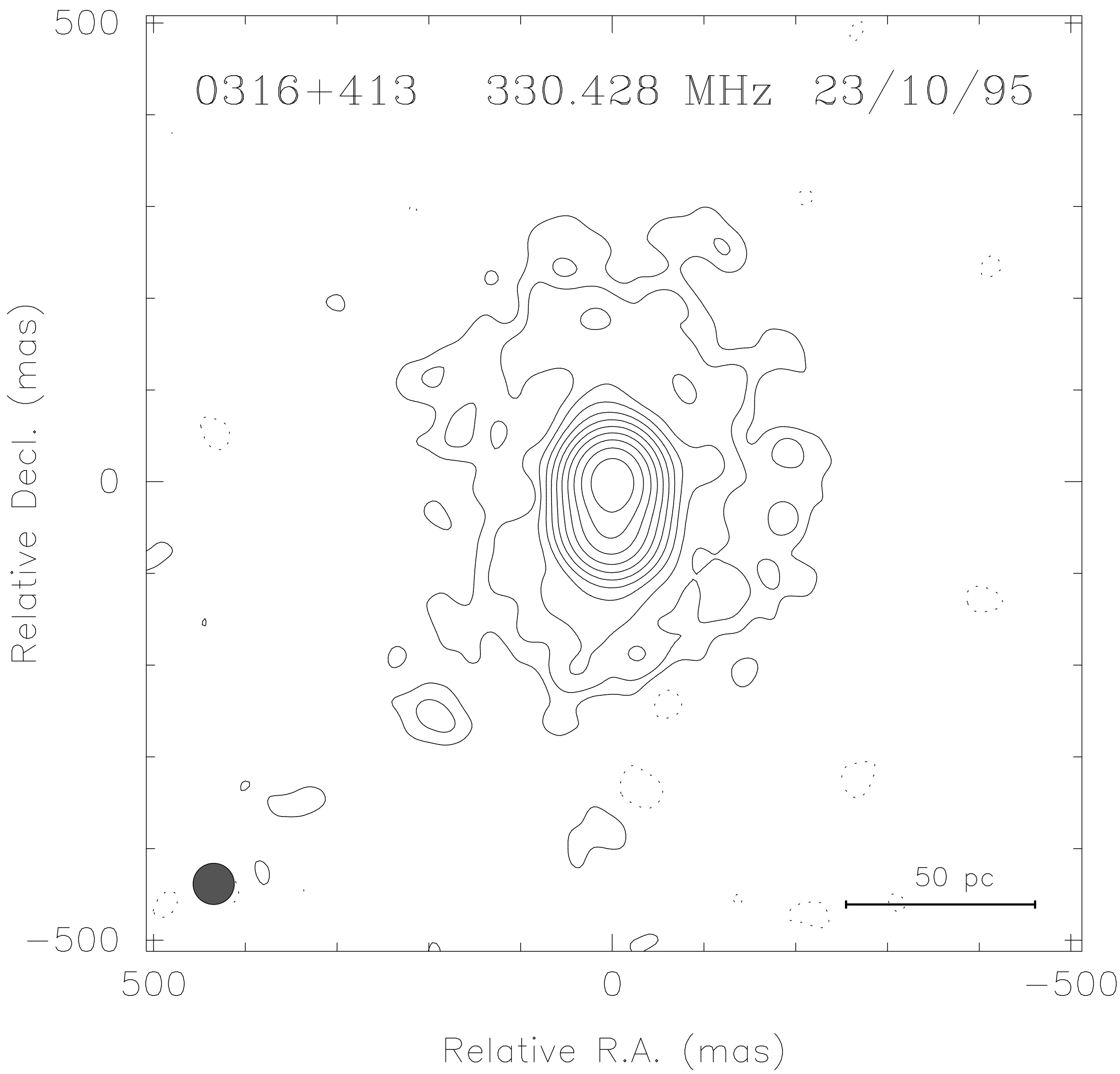

Fig. 4.— The naturally weighted and tapered image of 3C 84 at 330 MHz. A Gaussian taper falling to 50% at 4 Mλ was applied and the image was restored with a circular 45 mas beam. Contour levels are at −2, 2, 4, 8, 16, ... 2048 mJy/beam with negative contours shown as dashed lines.

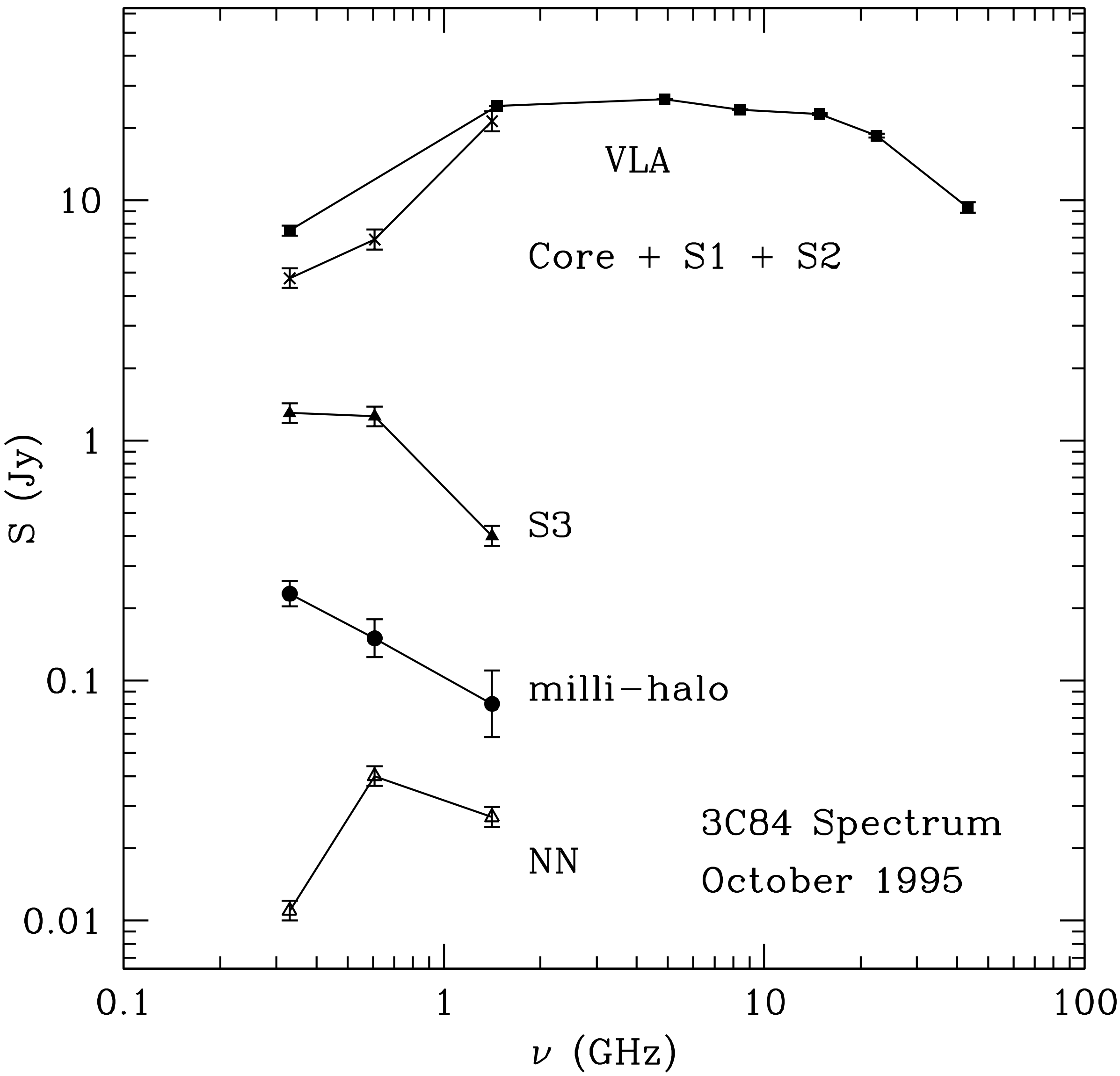

Fig. 5.— The integrated and component spectra of 3C 84. At the top is the VLA spectrum, observed 3 days before our VLBA run. Beneath that is our VLBA spectrum of the core components and of S3, and at the bottom is the VLBA spectrum of the milli-halo. The inset shows the spectrum of component NN. We assume an error of 10% in our amplitude calibration of the VLBA data.